Dynamic rewiring in small world networks

J. P. L. Hatchett,[1,*] N. S. Skantzos,[2,†] and T. Nikoletopoulos[3,‡]
[1]*Laboratory for Mathematical Neuroscience, RIKEN Brain Science Institute, Saitama 351-0198, Japan*
[2]*Instituut voor Theoretische Fysica, Celestijnenlaan 200D, K.U. Leuven B-3001, Belgium*
[3]*Department of Mathematics, King's College London, Strand WC2R 2LS, United Kingdom*
(Received 9 August 2005; published 5 December 2005)

We investigate equilibrium properties of small world networks, in which both connectivity and spin variables are dynamic, using replicated transfer matrices within the replica symmetric approximation. Population dynamics techniques allow us to examine the order parameters of our system at total equilibrium, probing both spin and graph statistics. Of these, interestingly, the degree distribution is found to acquire a Poisson-like form (both within and outside the ordered phase). Comparison with Glauber simulations confirms our results satisfactorily.

DOI: 10.1103/PhysRevE.72.066105 PACS number(s): 89.75.−k, 05.20.−y, 75.10.Nr

I. INTRODUCTION

Small worlds are systems characterized by a local neighborhood (given by short-range bonds) with a sparse set of long-range connections per spin. This simple architectural effect has been shown to bring about remarkable cooperative and synchronization phenomena. The term "small world" was coined by the now famous experiment by the Harvard social psychologist Stanley Milgram [1]. In 1967, as part of his research on the network of acquaintances in the United States, he took a number of letters and handed them over to people totally unrelated to the addressees, with instructions to pass them over to someone they thought might know the addressee. This process was repeated until the letters finally arrived at their destinations. Milgram then estimated the average path length from two randomly chosen individuals, which turned out to be a mere six. This experiment revealed that although social networks are very sparse, in reality any two pair of nodes can be topologically very close. In fact, numerical studies of other types of real networks (e.g., citation, linguistic, disease spreading, etc.) show that the small-world effect is a common architecture among real network structures and brings about optimal information processing. The question then arises, how do networks spontaneously evolve from (almost) random configurations into particular structures such as small-world ones? And which underlying process drives the distribution of the long-range shortcuts within the nodes? The above questions fall under a particularly active area of research, namely the evolution of networks (see, e.g., [2,3], or [4], for recent reviews). Since real networks (be they biological, social, economic, or otherwise) hardly ever maintain a static architecture, this problem of predicting network structure has important applications. In this paper we attempt to formulate and describe the thermodynamics of the problem from an analytic point of view. This carries the obvious set of advantages and disadvantages: while resulting in robust and exact results, it will be amenable to a set of (perhaps not fully realistic) assumptions. To be precise, we examine a coupled system on a small-world architecture in which both nodes and connections are mobile. However, the two dynamic processes occur on distinct time scales; connections are assumed to evolve slowly enough such that, at each of their update steps, spins have effectively reached equilibrium. This will allow us to avoid solving the explicit dynamical relations and instead turn directly to the thermodynamics. Our starting point is the free energy per connection degree of freedom. We couple the two dynamic processes of the spins and the connections by constructing two Hamiltonians: a typical Ising one describing the energy of the spins and a Hamiltonian of the connections, constructed to reward network configurations minimizing the free energy of the spins. This choice allows us to proceed analytically while retaining a sufficient amount of realism. The result is a replica theory where the replica dimension represents the ratio between the two temperatures (of the spins vs connection processes) [5,6].

Our paper is organized as follows: In the following section we introduce our model and the pair of energy functions describing the thermodynamics of the spins and the graph variables. In Sec. III we write the total free energy of the system as an extremization problem in terms of the typical finite-connectivity order parameter function. We then proceed to define the observables of our system, of which there are here two kinds, probing spin (Sec. IV A) and graph (Sec. IV B) organization statistics, respectively. The replica symmetric approximation (Sec. V) allows us to deal with the resulting replicated transfer matrices following the diagonalization process of [7,8]. We first derive in Sec. V A numerically tractable forms for our set of order functions which are to be solved via population dynamics. We perform a bifurcation analysis and plot phase diagrams showing the transition lines between ordered and paramagnetic phases in Sec. V B. Observables such as magnetization, average connectivity, or degree distribution then follow easily, see Sec. V C. We find that, perhaps contrary to initial expectations, the resulting degree distributions are close to, or exactly, Poisson. Comparison with numerical simulations shows good agreement

*Electronic address: hatchett@brain.riken.jp
†Electronic address: Nikos.Skantzos@fys.kuleuven.be
‡Electronic address: theodore@mth.kcl.ac.uk

given the complexity of these experiments requiring adiabatic (practically infinitely long) time scales.

II. MODEL DESCRIPTION

We study a system of N Ising spins $\boldsymbol{\sigma}=(\sigma_1,\ldots,\sigma_N)$ with $\sigma_i\in\{-1,1\}$, arranged on a small-world structure. We represent this by a one-dimensional lattice with uniform nearest-neighbor interactions of strength J_0 and with randomly chosen sparse shortcuts of strength $J_{ij}\in\{-J,J\}$ that can connect any distant pairs of spins (i,j). We will consider that the coupling strength J_{ij} is independent of $|i-j|$, namely the distance between the pair of spins. For every $i\neq j$ we assign a variable c_{ij}, denoting whether a connection exists ($c_{ij}=1$) or not ($c_{ij}=0$), with $c_{ii}=0$. In the absence of shortcuts the average path length is $N/4$, while in the combined system the scaling is bounded above by $\log(N)$. This significant reduction in the path length is commonly termed the "small-world effect" [9]. For static architectures, in which the link and bond matrices $\{c_{ij},J_{ij}\}$ are taken as quenched random variables, frustration effects are known to induce spin-glass phases [8].

Our model aims to examine the thermodynamic properties of the above spin systems under the freedom of allowing the connectivity and bond matrices $\{c_{ij},J_{ij}\}$ to evolve in time in search of the state that best promotes order within the system. To be precise, on short time scales the links and bonds can be seen as static variables with respect to which the spins equilibrate, while on longer time scales c_{ij} and J_{ij} explore their configuration space. The measure of this latter process is related to the ordering within the spin system on the instantaneous state of the graph. Thus the spins and the graph architecture on which they live are dynamically interwoven. It is quite natural that the architecture dynamics depends on the entire system state (including the spins) rather than just the architecture itself (as with, e.g., preferential attachment [10]). Links and connectivities are taken here to evolve on identical time scales, although generalizing this to more involved scenarios is also possible. On the time scale in which spins reach thermal equilibrium, our combined system is described by the "fast" Hamiltonian

$$H_f(\boldsymbol{\sigma},\mathbf{c},\mathbf{J})=-J_0\sum_i\sigma_i\sigma_{i+1}-\sum_{i\leqslant j}\sigma_iJ_{ij}c_{ij}\sigma_j \tag{1}$$

(where we take periodic boundary conditions on the chain). Spins equilibrate with respect to (1) at a temperature $T_f=1/\beta_f$ (we assume that the Boltzmann constant $k_B=1$), and their behavior is described by the partition function

$$Z_f(\mathbf{c},\mathbf{J})=\sum_{\boldsymbol{\sigma}}e^{-\beta_fH_f(\boldsymbol{\sigma},\mathbf{c},\mathbf{J})}. \tag{2}$$

On time scales sufficiently long to guarantee that spins have reached equilibrium, links and bonds are not static, but evolve dynamically and we will take their stationary state to be described by the "slow" Hamiltonian

$$H_s(\mathbf{c},\mathbf{J})=-\frac{1}{\beta_f}\log Z_f(\mathbf{c},\mathbf{J})+V(\mathbf{c},\mathbf{J}), \tag{3}$$

$$V(\mathbf{c},\mathbf{J})=\frac{1}{\beta_s}\sum_{i<j}c_{ij}\left[\log\left(\frac{N}{c}\right)+\log\cosh(K_pJ)-K_pJ_{ij}\right]. \tag{4}$$

This choice energetically favors those configurations of $\{c_{ij},J_{ij}\}$ that minimize the free energy of the spins. The role of the chemical potential $V(\mathbf{c},\mathbf{J})$ is twofold: first, it aims to preserve the overall nature of the small world system and it guarantees that for $N\to\infty$ the average number of connections per spin is a finite number. Second, it allows us to tune the relative concentration of $\{-J,J\}$ bonds in the system. These two roles of the chemical potential can be described by observables such the average number of connections and the average number of ferromagnetic bonds and are controlled by the parameters $c\in(0,\infty)$ and $K_p\in(-\infty,\infty)$, respectively. To understand the precise way in which this occurs one must add suitable generating terms to the free energy and subsequently extract the relevant observables. As the exact dependence of the system's observables on the control parameters K_p and c will only be clear once the free energy is evaluated, we will postpone the discussion on the physical meaning of K_p and c until Sec. III and IV B. We only mention here that in the limit $n\to0,c$ becomes the average connectivity and K_p controls the bias in the bond distribution.

The connectivity and bond variables $\{c_{ij},J_{ij}\}$ equilibrate with respect to this slow Hamiltonian at inverse temperature β_s, leading to a total partition function

$$Z_s=\sum_{\mathbf{c},\mathbf{J}}e^{-\beta_sH_s(\mathbf{c},\mathbf{J})}=\sum_{\mathbf{c},\mathbf{J}}[Z_f(\mathbf{c},\mathbf{J})]^{\beta_s/\beta_f}e^{-\beta_sV(\mathbf{c},\mathbf{J})}. \tag{5}$$

This partition function, by construction, contains $n=\beta_s/\beta_f$ replicas of the fast system. In general, the ratio of inverse temperatures n can take any value (integer or otherwise), so that analytic continuation in the replica dimension depends solely on our choice of temperature values. The limit $n\to0$ corresponds to temperatures $T_s\to\infty$ in which the partition sum (5) is dominated by the entropy of the slow system. Such coupled dynamic processes, which by construction admit an exact analytic solution, have been introduced in Refs. [5,6]. In contrast, $T_s\to0$ favors those architectures $\{c_{ij},J_{ij}\}$ that increase order among the spin variables for a given number of links. Note that this is a general optimization criterion which does not enforce *a priori* any particular structure on the links but allows the links to arrange themselves. In fact, the graph statistics become interesting observables, which we can measure, rather than enforced constraints. Our order parameters follow from the slow free energy per spin

$$f_s=-\lim_{N\to\infty}\frac{1}{\beta_sN}\log Z_s \tag{6}$$

and derivatives of this generating function.

III. THE FREE ENERGY

To calculate the slow partition function (5) we first take the trace over the connectivity and bond variables $\{c_{ij},J_{ij}\}$

$$Z_s = \sum_{\boldsymbol{\sigma}_1 \cdots \boldsymbol{\sigma}_N} e^{\beta_f J_0 \sum_i \boldsymbol{\sigma}_i \cdot \boldsymbol{\sigma}_{i+1}} \prod_{i<j} \left[1 + \frac{c}{N} \langle e^{\beta_f J \boldsymbol{\sigma}_i \cdot \boldsymbol{\sigma}_j} \rangle_J \right] \quad (7)$$

up to irrelevant multiplicative constants. We denote $\boldsymbol{\sigma}_i = (\sigma_i^1, \ldots, \sigma_i^n)$, where $\boldsymbol{\sigma}_i \cdot \boldsymbol{\sigma}_j = \Sigma_\alpha \sigma_i^\alpha \sigma_j^\alpha$ and define the abbreviation $\langle f(J) \rangle_J = rf(J) + (1-r) f(-J)$, and the probability $r \equiv [2 \cosh(K_p J)]^{-1} e^{K_p J}$. For $K_p \to \infty$, one has $r=1$. In this case all bonds in the system are strictly ferromagnetic at any given time. On the other hand, for $K_p \to -\infty$, one has $r=0$, and all bonds in the system are strictly antiferromagnetic at any given time. Thus, we see that the role of the parameter K_p is to control the ratio of ferromagnetic/antiferromagnetic couplings. With a modest amount of foresight we can anticipate from (4) that the limit $c \to \infty$ will lead to a densely connected system [this is indeed the case as we explicitly show later in Eq. (35)]. As we are interested in small-world structures, we will consider that the control parameter c is finite, and hence $c/N \to 0$ in the limit $N \to \infty$, so that the above product (7) can alternatively be seen as a product over exponentials [up to terms of $O(N^{-2})$]. We thus encounter the typical nested exponential form of finite connectivity problems. To achieve site factorization it is convenient to introduce into our expressions the order parameter function [11,12]

$$P(\boldsymbol{\sigma}) = \frac{1}{N} \sum_i \delta_{\boldsymbol{\sigma}, \boldsymbol{\sigma}_i} \quad (8)$$

via appropriately defined delta functions, which is a probability distribution over replicated spins. In the limit $N \to \infty$ we can now evaluate the free energy (6) via the steepest descent and express it as an extremization problem in the space of probability distributions $P(\boldsymbol{\sigma})$, namely,

$$f_s = \mathrm{extr}_{\{P(\boldsymbol{\sigma})\}} \left\{ \frac{c}{2\beta_s} \sum_{\boldsymbol{\sigma}\boldsymbol{\sigma}'} P(\boldsymbol{\sigma}) P(\boldsymbol{\sigma}') \langle e^{\beta_f J \boldsymbol{\sigma} \cdot \boldsymbol{\sigma}'} \rangle_J - \lim_{N \to \infty} \frac{1}{\beta_s N} \log \sum_{\boldsymbol{\sigma}_1 \cdots \boldsymbol{\sigma}_N} \prod_i T_{\boldsymbol{\sigma}_i, \boldsymbol{\sigma}_{i+1}}[P] \right\}, \quad (9)$$

where $T_{\boldsymbol{\sigma},\boldsymbol{\sigma}'}[P]$ represent the transfer matrix elements

$$T_{\boldsymbol{\sigma},\boldsymbol{\sigma}'}[P] = \exp\left[\beta_f J_0 \boldsymbol{\sigma} \cdot \boldsymbol{\sigma}' + c \sum_{\boldsymbol{\tau}} P(\boldsymbol{\tau}) \langle e^{\beta_f J \boldsymbol{\sigma} \cdot \boldsymbol{\tau}} \rangle_J \right], \quad (10)$$

and $P(\boldsymbol{\sigma})$ is to be evaluated from the fixed-point equation

$$P(\boldsymbol{\sigma}) = \frac{\mathrm{Tr}(Q[\boldsymbol{\sigma}] T^N[P])}{\mathrm{Tr}(T^N[P])} \quad Q_{\boldsymbol{\sigma},\boldsymbol{\sigma}'}[\boldsymbol{\tau}] \equiv \delta_{\boldsymbol{\sigma},\boldsymbol{\tau}} \delta_{\boldsymbol{\sigma},\boldsymbol{\sigma}'}. \quad (11)$$

For more details on the derivation of the above expressions we refer the reader to Ref. [8] where the special case of the limit $n \to 0$ was studied.

Finding solutions of (11) amounts to diagonalizing the transfer matrix T of dimensionality $2^n \times 2^n$. This problem has been solved in Ref. [7]. Here we will not be concerned in the entire spectrum of eigenvalues, as the limit $N \to \infty$ ensures that only the largest eigenvalue λ_0 will provide a nonvanishing contribution to the free energy. The left and right eigenvectors associated with this eigenvalue follow from the equations

$$\sum_{\boldsymbol{\sigma}'} T_{\boldsymbol{\sigma},\boldsymbol{\sigma}'}[P] U(\boldsymbol{\sigma}') = \lambda_0 U(\boldsymbol{\sigma}), \quad (12)$$

$$\sum_{\boldsymbol{\sigma}'} V(\boldsymbol{\sigma}') T_{\boldsymbol{\sigma}',\boldsymbol{\sigma}}[P] = \lambda_0 V(\boldsymbol{\sigma}). \quad (13)$$

These eigenvectors are unique up to the usual arbitrary multiplicative factor and are non-negative [7,13]. We note that we need both left and right eigenvectors since the transfer matrix $T[P]$ is nonsymmetric. The order function $P(\boldsymbol{\sigma})$ (8) is manifestly normalized. Due to our scaling freedom for the eigenvectors we can always choose them so that $\Sigma_{\boldsymbol{\sigma}} U(\boldsymbol{\sigma}) = \Sigma_{\boldsymbol{\sigma}} V(\boldsymbol{\sigma}) = 1$. The physics of our system is given by the normalized distributions $P(\boldsymbol{\sigma}), V(\boldsymbol{\sigma}), U(\boldsymbol{\sigma})$, which are to be found by self-consistently solving Eqs. (10)–(13). In fact, $U(\boldsymbol{\sigma})$ and $V(\boldsymbol{\sigma})$ turn out to represent the distributions of cavity spins with a chain bond rather than a graph bond removed [13].

IV. OBSERVABLES

A. Spin system observables

We are interested in probing the organizational properties of our system both within the spin variables and the connectivity ones. For the spin system, we define the canonical observables; the magnetization and the overlap order parameter as moments of the probability distribution (8), namely,

$$m_\alpha = \sum_{\boldsymbol{\sigma}} P(\boldsymbol{\sigma}) \sigma^\alpha, \quad (14)$$

$$q_{\alpha\beta} = \sum_{\boldsymbol{\sigma}} P(\boldsymbol{\sigma}) \sigma^\alpha \sigma^\beta. \quad (15)$$

In the above pair of equations and henceforth, the quantities $P(\boldsymbol{\sigma}), V(\boldsymbol{\sigma})$, and $U(\boldsymbol{\sigma})$ are given by their saddlepoint values.

It is well known that infinite dimensional systems, such as small world lattices, with frozen bonds of random signs, will have a spin-glass ground state at low temperatures for certain values of the control parameters [14–16]. This spin-glass ordering is intimately linked to frustration within the system; the inability of spins to find energetically optimal configurations. By allowing the architecture some limited degree of freedom, we expect that the system will be able to optimize its state somewhat better. Probing the degree of frustration within the system as the slow temperature is varied is an interesting problem. The frustration is normally defined as the fraction of closed loops from sites $i_1 \to i_2 \to \cdots i_k \to i_1$, where the product $J_{i_1 i_2} \cdots J_{i_k i_1}$ is negative. Unfortunately, to measure this directly in our system where bonds are mobile, would require us to be able to measure correlations over long length scales within the system [in fact, scaling like the average loop length $\sim \log(N)$], which is technically difficult. To try to finesse this problem, as in Refs. [17,18], the fraction of misaligned spins was calculated, i.e., the fraction of spins that did not point in the direction of their local field. Due to the mobility of the connections in our system, we expect that thermal equilibrium states within the ordered phases will be steered toward configurations where spin alignment with

their local fields is optimal. The result of this structural organization can be measured by the quantity $\phi = \int_{-\infty}^{0^-} dh\, P(1,h) + \int_{0^+}^{\infty} dh\, P(-1,h)$, which gives the fraction of misaligned spins and is defined in terms of the joint spin-field distribution

$$P(\sigma,h) = \lim_{N\to\infty} (1/N) \sum_i \langle \delta_{\sigma,\sigma_i} \delta[h - h_i(\boldsymbol{\sigma})] \rangle_s,$$

where $\langle \cdots \rangle_s$ denotes thermal averages over the slow process $\langle x \rangle_s = Z_s^{-1} \Sigma_{\mathbf{c},\mathbf{J}} e^{-\beta_s H_s(\mathbf{c},\mathbf{J})} x$, and $h_i(\boldsymbol{\sigma}) \equiv \Sigma_j c_{ij} J_{ij} \sigma_j + J_0(\sigma_{i+1} + \sigma_{i-1})$ denotes the local field at site i. However, at, e.g., very low temperatures, one expects the spins to align to their local fields whether they are in a spin-glass phase or not. Thus, to try to get a different measure to probe the frustration in the system we consider the fraction of bonds in the graph, which is not energetically optimized by the spin configuration

$$\psi = \frac{1}{N} \sum_i \langle \Theta(-\sigma_i \sigma_{i+1} J_0) \rangle_s + \frac{1}{cN} \sum_{i<j} \langle c_{ij} \Theta(-\sigma_i \sigma_j J_{ij}) \rangle_s. \tag{16}$$

This is also not an absolute measure of frustration, but in the low temperature spin-glass phase ψ will be nonzero, as opposed to a low temperature ferromagnet where we would have $\psi = 0$. The calculation of either ψ or ϕ is similar to the calculation of the free energy, with a specific observable (i.e., matrix in the transfer matrix notation) at one or two sites. We find

$$\psi = D_1 \sum_{\boldsymbol{\sigma}\boldsymbol{\sigma}'} V(\boldsymbol{\sigma}) \Theta(-\sigma_1 \sigma'_1 J_0) T_{\boldsymbol{\sigma}\boldsymbol{\sigma}'}[P] U(\boldsymbol{\sigma}') + D_2 \sum_{\boldsymbol{\sigma}\boldsymbol{\sigma}'} P(\boldsymbol{\sigma}) P(\boldsymbol{\sigma}') \langle \Theta(-\sigma_1 \sigma'_1 J) e^{\beta_f J \boldsymbol{\sigma}\cdot\boldsymbol{\sigma}'} \rangle_J, \tag{17}$$

where D_1 and D_2 are normalization constants to give the fraction of sites, i.e., $D_1 = \Sigma_{\boldsymbol{\sigma}\boldsymbol{\sigma}'} V(\boldsymbol{\sigma}) T_{\boldsymbol{\sigma}\boldsymbol{\sigma}'}[P] U(\boldsymbol{\sigma}')$ and $D_2 = \Sigma_{\boldsymbol{\sigma}\boldsymbol{\sigma}'} P(\boldsymbol{\sigma}) P(\boldsymbol{\sigma}') \langle e^{\beta_f J \boldsymbol{\sigma}\cdot\boldsymbol{\sigma}'} \rangle$.

B. Connectivity system observables

Let us now inspect organizational phenomena within the graph. We first identify the roles played by the control parameters c and K_p that appear in the chemical potential (4). This can be done by adding suitable generating terms into the Hamiltonian (3) and monitoring their impact on (9). For instance, if one transforms $H_s \to H_s + \lambda(1/c)\Sigma_{i<j} c_{ij}$, then taking derivatives $(\partial f_s / \partial \lambda)|_{\lambda=0}$ translates to

$$\bar{c} \equiv \frac{1}{N} \sum_{ij} \langle c_{ij} \rangle_s = c \sum_{\boldsymbol{\sigma}\boldsymbol{\tau}} P(\boldsymbol{\sigma}) P(\boldsymbol{\tau}) \langle e^{\beta_f J \boldsymbol{\sigma}\cdot\boldsymbol{\tau}} \rangle_J. \tag{18}$$

Now $\bar{c}$ represents the average number of connections per spin in our system. It depends on the replica dimension n via the scalar spin product and it reduces to $\bar{c} = c$ in the limit $n \to 0$. In the limit $c \to \infty$ [scaling J as J/c to keep the local fields in the graph $h_i^{\mathrm{gr}}(\boldsymbol{\sigma}) \equiv \Sigma_j c_{ij} J_{ij} \sigma_j$ of $O(1)$] we again recover $\bar{c} = c$ to leading order as found in [17]. Similarly to the above, one also finds that taking $H_s \to H_s + \lambda \Sigma_{i<j} c_{ij} J_{ij}$ produces the average bond strength on the graph. As well as being interested in the above average connectivity and bond strength at total equilibrium, we would also like to investigate the connectivity structure in more detail. To make contact with a variety of recent work on complex networks [4,19] we define the degree distribution for our system

$$\Xi(k) = \lim_{N\to\infty} \frac{1}{N} \sum_i \left\langle \delta_{k, \sum_j c_{ij}} \right\rangle_s. \tag{19}$$

Following a calculation similar to that of the free energy in Sec. III one finds that

$$\Xi(k) \sim \int \frac{d\hat{k}}{2\pi} e^{ik\hat{k}} \sum_{\boldsymbol{\sigma}\boldsymbol{\sigma}'} V(\boldsymbol{\sigma}) U(\boldsymbol{\sigma}') \exp\left[c \sum_{\boldsymbol{\tau}} \langle P(\boldsymbol{\tau}) e^{\beta_f J \boldsymbol{\sigma}\cdot\boldsymbol{\tau} - i\hat{k}} \rangle_J + \beta_f J_0 \boldsymbol{\sigma}\cdot\boldsymbol{\sigma}' \right]. \tag{20}$$

We have absorbed the normalization constant of the above distribution in the symbol $\sim$ (we will repeatedly use this short-hand notation from this point onwards). The above observables are all expressed in terms of the trio of distributions $P(\boldsymbol{\sigma}), V(\boldsymbol{\sigma})$, and $U(\boldsymbol{\sigma})$, taken at the saddle point of the free energy (9). To proceed with a numerical evaluation of the observables one now needs to specify a form for these densities.

V. REPLICA SYMMETRY AND TRANSFER-MATRIX DIAGONALIZATION

To solve the self-consistent Eqs. (11)–(13) one is required to make certain assumptions. These equations represent different distributions over replicated spins (for any $n \in \mathbb{R}$). We will consider the simplest possible scenario in which permutation of spins within different replica groups $\alpha = 1, \ldots, n$ leave the order functions invariant (replica symmetry).

For any natural $n \in \mathbb{N}^+$ it is relatively straightforward to express these distributions, as their support is a finite discrete set. For the more general case of $n \in \mathbb{R}$ one has to make an analytic continuation which leads to more complicated expressions. For the sake of clarity we will presently restrict ourselves to $n \in \mathbb{R}$. A detailed analysis of the special case of $n \in \mathbb{N}$ can be found in Appendix I.

For any real n we require

$$X(\boldsymbol{\sigma}) = \int dz\, x(z) \prod_{\alpha=1}^{n} \frac{e^{z\sigma_\alpha}}{[2\cosh(z)]}. \tag{21}$$

This ansatz holds for any distribution $X(\boldsymbol{\sigma})$ and in particular as $X \in \{P, U, V\}$ we define the ansatz in terms of the densities $x \in \{p, u, v\}$. Normalization requires $\int dz\, x(z) = 1$.

Note that for any $n \in \mathbb{N}^+$ one can in principle solve Eqs. (11)–(13) without making any assumption about the structure of the replica space (symmetric or otherwise): for integer n, the vectors $\boldsymbol{\sigma}$ retain a well-defined dimensionality and the diagonalization of the matrix (10) is a straightforward, albeit tedious, problem. This approach is therefore a good test of the validity of the replica symmetric approximation. However, as we will see shortly, imposing replica symmetry in

our equation leads to computational costs of $O(n)$ instead of $O(2^n)$, which is the result of the above "exact" approach. Therefore, only relatively small values of n are practically feasible. Furthermore, we know that for $n=1$, the order function can trivially be written as $P(\boldsymbol{\sigma})=P(\Sigma_\alpha \sigma_\alpha)$, which implies that replica symmetry is in this case exact. For higher values of n, we do not expect violation of the replica symmetry as the spin system is embedded in a higher temperature bath than for $n=1$. If this is true, then our solution is exact for $n \in \mathbb{N}^+$.

A. Self-consistent order function equations

In this section we aim to derive a closed set of equations for the trio of densities $\{p,u,v\}$. First, a Taylor expansion of the transfer matrix elements (10) into a series of exponentials and insertion of the replica symmetric ansatz (21) leads to

$$T_{\boldsymbol{\sigma},\boldsymbol{\sigma}'}[P] = e^{\beta_f J_0 \boldsymbol{\sigma}\cdot\boldsymbol{\sigma}'} \langle e^{\beta_f \theta \Sigma_\alpha \sigma_\alpha} \rangle_\theta, \tag{22}$$

with $\langle \cdots \rangle_\theta$ representing averages over the measure

$$M(\theta|n = \sum_{k\geqslant 0} \frac{e^{-c}c^k}{k!} \left\langle \int \left[\prod_{l\leqslant k} \frac{dh_l p(h_l)}{[2\cosh(h_l)]^n} \right] \times e^{n\Sigma_l B(J_l,h_l)} \delta\left[\theta - \sum_{l\leqslant k} A(J_l,h_l) \right] \right\rangle_{\{J_l\}}, \tag{23}$$

and where we introduce the functions

$$A(J,x) = a \tanh[\tanh(\beta_f J)\tanh(x)], \tag{24}$$

$$B(J,x) = \frac{1}{2}\log(4\cosh[\beta_f J + x]\cosh[\beta_f J - x]). \tag{25}$$

The latter of the above equations is related to the free energy shifts which occur during an iteration [16,20]. For $n\to 0$ and within replica symmetry, this second term does not contribute, although in the more general case of $n>0$ it will play an important role. Equation (24) can be identified as a "message" (or effective field) passed during *belief propagation*. This is an efficient algorithm that can solve inference problems on sparse graphs and is related to the Bethe approximation in statistical mechanics [21]. Following the belief propagation picture, one can also relate (23) to a weighted measure over the messages coming from the long range bonds. Performing the spin summations in (12) and (13) using the ansatz (21) and requiring the resulting expression to have the eigenvector form leads to

$$\lambda_0(n) u\left(x \middle| n\right) = \int dx' u\left(x' \middle| n\right) \frac{\cosh^n(x)}{\cosh^n(x')} \times \langle e^{nB(J_0,x')} \delta[x - \theta - A(J_0,x')] \rangle_\theta, \tag{26}$$

$$\lambda_0(n) v\left(y \middle| n\right) = \int dy' v\left(y' \middle| n\right) \frac{\cosh^n(y)}{\cosh^n(y')} \times \langle \mathrm{e}^{nB(J_0,y'+\theta)} \delta[y - A(J_0,y' + \theta)] \rangle_\theta, \tag{27}$$

so that the largest eigenvalue follows from the above by simple integration. To close the above equations we also need to derive an expression for the function $p(h)$. The starting point for this is Eq. (11). Rewriting the traces in terms of the eigenvectors and substituting our ansatz (21) results in

$$p(h) = \frac{\int dxdy\, u(x)v(y) \left\{ \frac{\cosh(h)}{2\cosh(x)\cosh(y)} \right\}^n \delta[h - (x+y)]}{\int dxdy\, u(x)v(y) \left\{ \frac{\cosh(x+y)}{2\cosh(x)\cosh(y)} \right\}^n}. \tag{28}$$

The coupled set of Eqs. (26)–(28) are to be solved self-consistently. They have a clear interpretation in terms of message-passing algorithms: $p(h)$ gives the distribution of messages passed along long-range shortcuts, whereas $u(x)$ and $v(y)$ give that of messages passed along the chain (from the left and right neighbors). The numerical solution of these equations follows along the lines of the population dynamics methodology of [20].

B. Phase diagrams

Having derived the main equations from which our observables follow, namely (26)–(28), we can now proceed to the evaluation of the transition lines in our phase diagram numerically and via a bifurcation analysis. First, we see that the state $p(x)=u(x)=v(x)=\delta(x)$ always solves Eqs. (26)–(28), giving $m=q=0$ for all temperatures. We can therefore associate this state with the high-temperature (paramagnetic) solution. To examine continuous bifurcations away from this solution we assume that close to the transition the fields are small, and that the paramagnetic δ distributions evolve to either a distribution of small, nonzero means (in leading order) marking the paramagnetic to ferromagnetic transition or to a distribution of small, nonzero variances (again in leading order) marking the paramagnetic to spin-glass (SG) transition. With these considerations in mind we define the moments $\overline{h^\ell}=\int dh\, p(h)h^\ell = O(\epsilon^\ell)$ for some $0<\epsilon \ll 1$ [and similarly for $\overline{x^\ell}=\int dx\, u(x)x^\ell$ and $\overline{y^\ell}=\int dy\, v(y)y^\ell$]. We assume that there is no first order transition. Then, expanding Eqs. (26)–(28) for the small values of fields and using $\bar{h}=\bar{x}+\bar{y}$ and $\overline{h^2}=\overline{x^2}+\overline{y^2}$, which follows from (28) we arrive at paramagnetic to ferromagnetic and paramagnetic to spin-glass transition lines

$$P \to F: \quad 1 = c\langle \sinh(\beta_f J)\cosh^{n-1}(\beta_f J)\rangle_J e^{2\beta_f J_0}, \tag{29}$$

$$P \to \mathrm{SG}: \quad 1 = c\langle \sinh^2(\beta_f J)\cosh^{n-2}(\beta_f J)\rangle_J \cosh(2\beta_f J_0). \tag{30}$$

These equations reduce to those found in Ref. [8] in the limit $n\to 0$, recovering the small-world bifurcations. The correspondence is exact if we identify the paramagnetic mean connectivity here with c. It also reduces to those of Ref. [18] for $J_0=0$ and $r=1$ (where r was defined in Sec. III and represents the probability of any given bond to be ferromagnetic). For these parameters, the model of Ref. [18] is a Hopfield model on a dynamic random graph with a single

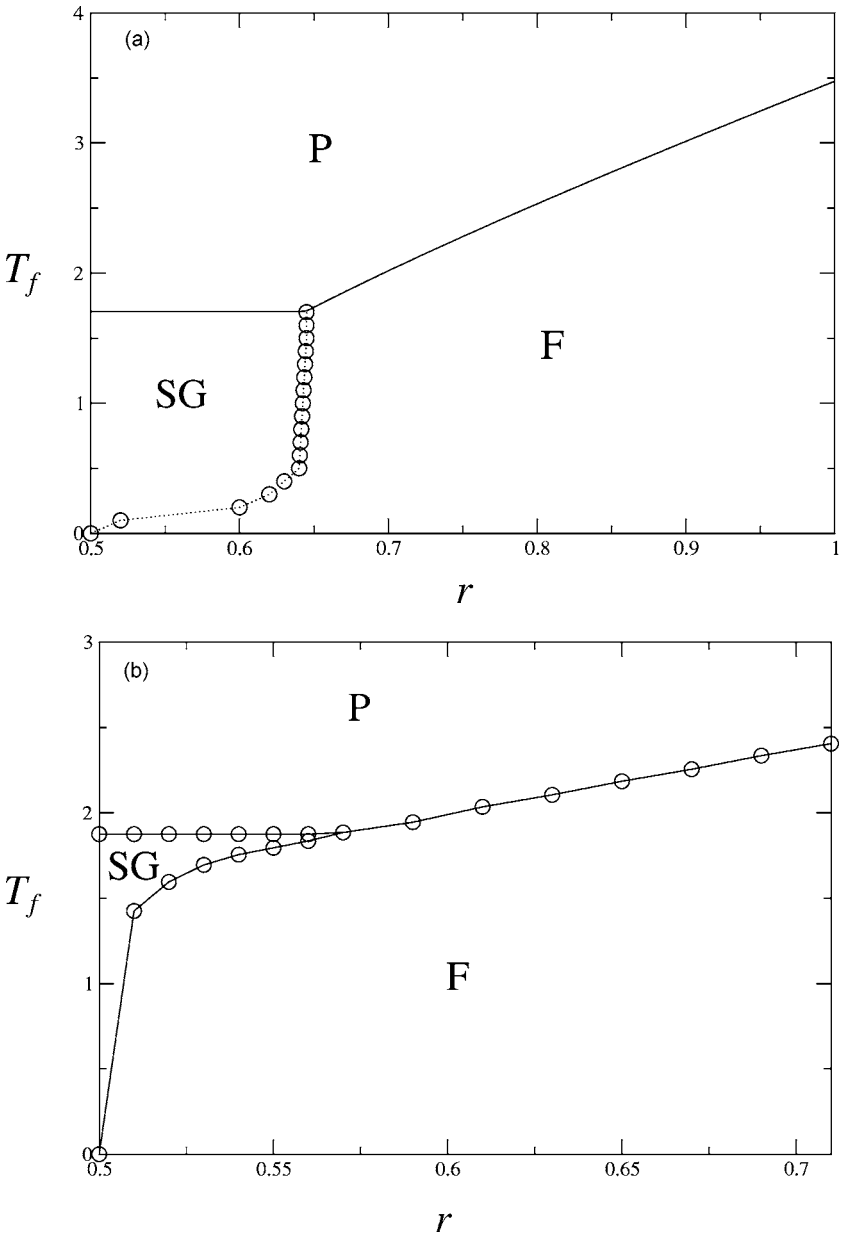

FIG. 1. We plot the phase diagrams for $c=2$ and $J=J_0=1$. Panel (a) is for $n=0.1$, where the solid lines are given by the bifurcation conditions (29) and (30), while the markers come from solving the order parameter equations numerically, and the dotted line linking markers is a guide to the eye. Panel (b) is for $n=2$ and all lines are linking markers which come from solving the order parameter equations numerically. The $P\rightarrow F$ and $P\rightarrow$ SG transitions are here first order. For larger values of n, we see that the links are better able to align to increasing order. First, the transition temperature from the paramagnetic phase is higher and second, the size of the spin-glass phase is significantly smaller.

pattern stored (in this scenario the Hopfield model becomes equivalent to a ferromagnet with a different gauge). It is well known for these models [18] that as n increases, the transitions are increasingly likely to be of first order. Thus, to produce phase diagrams of the system, as well as looking at the bifurcation lines given by the above, we also solved the full equations numerically. Results are shown in Fig. 1 where we see that increasing n decreases the size of the spin-glass phase, which we expect is due to the increased cooperativity.

C. Observables within replica symmetry

Let us now express our observables in terms of the densities $\{p,u,v\}$ and within replica symmetry. First, the magnetization (14) and overlap (15) order parameters become

$$m=\int dh\, p(h)\tanh(h), \tag{31}$$

$$q=\int dh\, p(h)\tanh^2(h), \tag{32}$$

so that given the stationary profile of p from the self-consistent Eqs. (26)–(28) we may evaluate any of the above. In Fig. 2 we plot the magnetization for two different values of n, and compare our results against simulation experiments. More details on the simulations are given in Sec. VI B. Let us note here that due to the coupled dynamical processes, these experiments are particularly time consuming so that only modest system sizes are allowed within reasonable CPU cost. Within these constrains we feel that the agreement is reasonable.

Evaluating the fraction of energetically nonoptimal bonds ψ is slightly more involved. The replica symmetric transfer matrix is given by

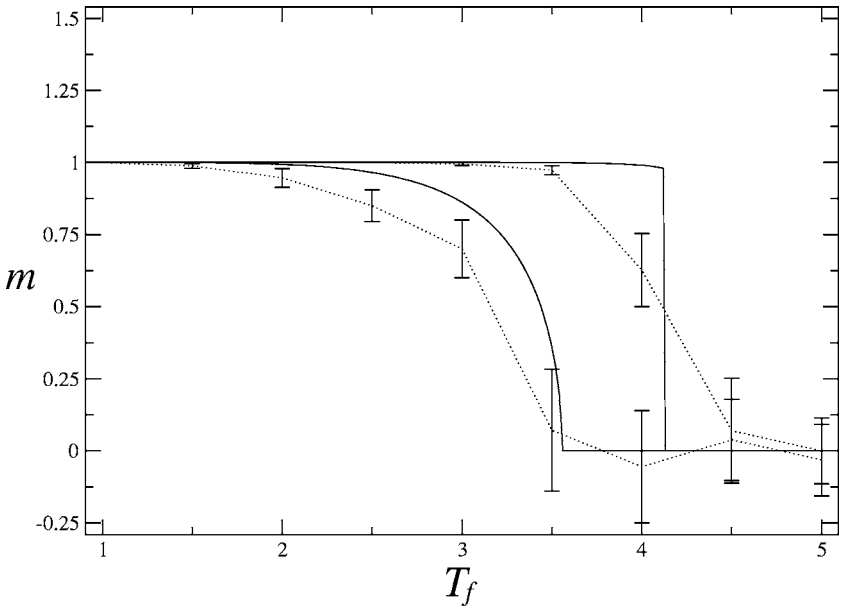

FIG. 2. We plot the magnetization m as a function of temperature T_f for $n=1$ (lower lines) and $n=5$ (upper lines). The solid lines are the theoretical predictions. Dotted lines are a guide for the eye, joining the markers with error bars which come from simulations. For the coupling strengths we have taken $J_0=J=1$, while for the control parameters we have chosen $c=2$, and $K_p=\infty$ [equivalently, the probability of a bond to be ferromagnetic $r=e^{K_p J}/2\cosh(K_p J)=1$]. The simulations were done via Monte Carlo Glauber dynamics on $N=200$ spins, see Sec. VI B for details. Despite the small system size they seem to be in reasonable agreement with the theory.

$$T_{\boldsymbol{\sigma},\boldsymbol{\sigma}'}[P] = e^{\beta_f J_0 \boldsymbol{\sigma}\cdot\boldsymbol{\sigma}'} \int d\theta M(\theta) e^{\beta_f \theta \sum_\alpha \sigma_\alpha} \tag{33}$$

leading to

$$\psi = D_1 \int dx dy d\theta\, u(x) v(y) M(\theta) \times \frac{e^{-\beta_f J_0} 2\cosh(x+\theta-y)}{[e^{y} 2\cosh(x+\theta+\beta_f J_0) + e^{-y} 2\cosh(x+\theta-\beta_f J_0)]^{n-1}} + D_2 \int dh_1 dh_2 p(h_1) p(h_2) \times e^{-\beta_f J} \frac{r 2\cosh(h_1+h_2) + (1-r) 2\cosh(h_1-h_2)}{[e^{h_2} 2\cosh(h+\beta_f J) + e^{-h_2} 2\cosh(h-\beta_f J)]^{n-1}}. \tag{34}$$

We plot ψ for a few sets of parameters in Fig. 3. As the fast temperature goes to ∞, we have $\psi \to 1$, i.e., exactly half of the bonds at any point in time are energetically optimal, so in the high temperature phase the ordering is nonexistent (as one would expect). We also see that increasing n leads to better levels of optimization. This is again what one would expect, but it is possible to quantify it here. Decreasing the probability r (of any bond to be ferromagnetic) and hence increasing the disorder, makes it harder for the spins to energetically optimize themselves, although at low temperatures, due to the condensation phenomena in the bonds (see below), the magnetization will increase to 1. With all spins aligned, the fraction of energetically nonoptimal bonds becomes exactly the fraction of bonds with $J<0$. We see this in Fig. 3, as $T_f \to 0, \psi \to 1-r$. This would not be the case for a fully unbiased bond distribution $r=0.5$, where ferromagnetic ordering in the spins is ruled out for any value of n and T_f.

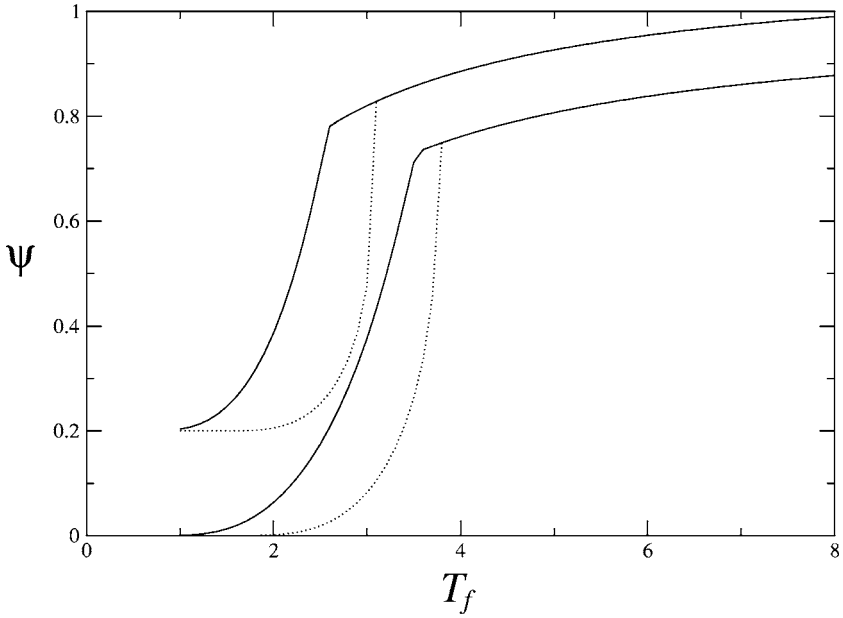

FIG. 3. We plot the fraction of misaligned bonds ψ against the temperature T_f. For the coupling strengths we have taken $J_0=J=1$, and the control parameter is $c=2$. The solid lines are for $n=1$, while the dotted lines are for $n=3$. The upper pair of lines are for $r=0.8$, while the lower pair are for the $r=1$, where r describes the probability of any bond within the graph to be ferromagnetic. We see that in the ordered phase, increasing n allows the system to optimize the bonds energetically.

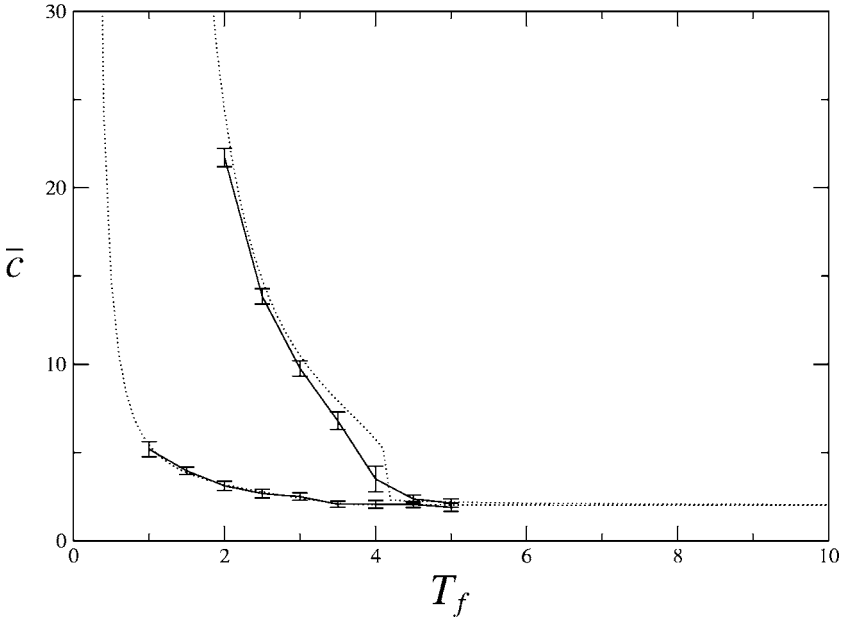

FIG. 4. We plot the average number of bonds $\bar{c}$ against the fast temperature (of the spin systems) for coupling strengths $J=J_0=1$, control parameter $c=2$, and $K_p=\infty$ (or $r=1$). The higher line with the first order transition is for $n=5$, while the lower line is for $n=1$. The dotted lines are the theoretical predictions, while the solid line is a guide for the eye linking the error bars which are measurements from simulation experiments. The agreement is reasonable although, as in Fig. 2, we find that the sharp transition is smeared out due to the small system size for over simulations ($N=200$ spins).

We now turn our attention to the graph observables. We first focus on the average connectivity, which is expressed as

$$\bar{c} = c \int dh_1 dh_2 p(h_1) p(h_2) \{\cosh(\beta_f J) + \tanh(h_1)\tanh(h_2)\sinh(\beta_f J)\}^n. \quad (35)$$

In Fig. 4 we plot $\bar{c}$ against T_f. We have taken $r=e^{K_p J}/2\cosh(K_p J)=1$, i.e., all bonds at any given point in the system are of uniform strength J with probability 1. At low temperatures (the specific temperature depends on other parameters), the average connectivity increases sharply. This is due to ordering within the spin system, leading to an increased energetic gain by adding connections. Higher values of n, for a given T_f, means a lower value of T_s and hence the connectivity variables will be governed more strictly by the free energy of the fast system, which is minimized by high connectivity configurations.

We also looked at the full degree distribution, which is given up to normalization constants by

$$\Xi(k) \sim \frac{c^k}{k!} \int \prod_{\ell \leqslant k} \left\{ \frac{dh_\ell dJ_\ell p(h_\ell) Q(J_\ell)}{[2\cosh(h_\ell)]^n} \right\} \frac{dxdy\, u(x)v(y)}{[4\cosh(x)\cosh(y)]^n} \times e^{n\sum_\ell B(J_\ell,h_\ell)+nB(J_0,x)} \times \left\{ 2\cosh\left[y + A(J_0,x) + \sum_\ell A(J_\ell,h_\ell) \right] \right\}. \quad (36)$$

A typical example of this degree distribution is given in Fig. 5. What is particularly interesting is that although the degree distribution is in principle free, to take on any form it keeps very close to that of the Poisson degree distribution with

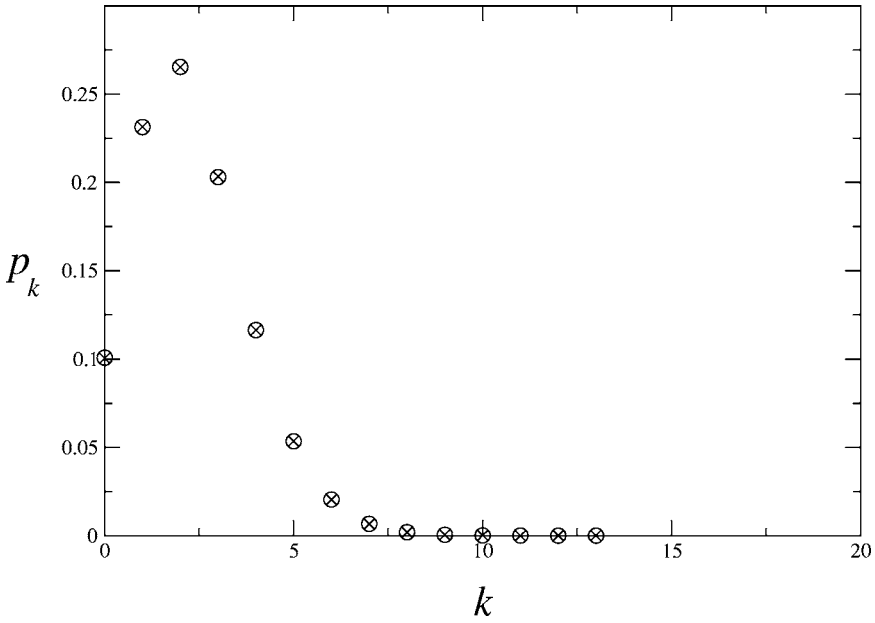

FIG. 5. We plot the probability that a given node has degree k, p_k against k for $n=0.5$, $r=0.6$, $T_f=J=J_0=1$, and $c=2$ within the spin-glass regime where other observable values are $m=0$ and $q\approx 0.581$. The true degree distribution is given by crosses, for comparison we have also given the Poisson distribution with the same value of $\bar{c}$ with circles. Although there are differences between the two, for this set of parameters the difference is very small.

mean $\bar{c}$. In fact, in the paramagnetic phase, we know that $P(\boldsymbol{\sigma})=2^{-n}$ and thus we find $\bar{c}$ exactly from (18) without invoking replica symmetry, namely $\bar{c}_{\mathrm{PM}}=c\cosh^n(\beta J)$, which is independent of r since cosh is an even function. Thus the average degree is independent of the bond disorder (in this model) in the paramagnetic phase. Here, the degree distribution also scales linearly with c. By using the fact that in the paramagnetic phase we also have $U(\boldsymbol{\sigma})=V(\boldsymbol{\sigma})=2^{-n}$, we can also see that $\Xi(k)=e^{-\bar{c}_{\mathrm{PM}}}\bar{c}_{\mathrm{PM}}^k/k!$, i.e., the degree distribution is exactly Poisson. We also find exact results in the fully ferromagnetic phase where $P(\boldsymbol{\sigma})=U(\boldsymbol{\sigma})=V(\boldsymbol{\sigma})=\Pi_\alpha\delta_{\sigma^\alpha,\sigma^1}$. There $\bar{c}_{\mathrm{FM}}=c\langle e^{\beta_f nJ}\rangle_J$, and $\Xi(k)=e^{-\bar{c}_{\mathrm{FM}}}\bar{c}_{\mathrm{FM}}^k/k!$. In both these cases the degree distribution is exactly Poisson. This can be understood on the basis that in both phases there is no energetic gain in having any particular $c_{ij}=1$, since it will not affect the spin distribution (they are either all set to be aligned or fully random) and thus the degree distribution will be the maximum entropy one, i.e., Poisson. It is also clear that there is a range of ordered states between the two extremes above. We cannot say anything further analytically about the degree distribution there, although it is possible to show that the degree distribution is not exactly a Poisson distribution. However, we may evaluate our order parameter equations numerically, and we find that although the degree distribution is not Poisson, it is very close, as shown in Fig. 5. It was not obvious that this should be the case, and indeed, the increased critical temperature for a scale free degree distribution would have suggested that this could be optimal, since it increases ordering, but it transpires that this does not occur here.

VI. POPULATION DYNAMICS AND SIMULATIONS

In this section we briefly discuss issues related to the numerical solution of the equations and further particulars on the implementation of the simulation experiments.

A. Population dynamics

The trio of self-consistent Eqs. (26)–(28) has been solved with the population dynamics method of [20]. The main difference is that one is now required to weight the averages of the field distributions by an n-dependent factor. In practice, expressions of the form $\phi(x')=\int dx\ \phi(x)w(x)\delta[x'-g(x)]$, for some arbitrary probability density $\phi(x)$, weight $w(x)$, and updating function $g(x)$, are solved by sampling values of x from the density $\phi(x)$ and updating $x'\to g(x)$ with weight $w(x)$. To interpret this weighting term, one can write $w(x)=\lfloor w(x)\rfloor+p$, where $\lfloor w(x)\rfloor$ is the integer part of $w(x)$, and p is the fractional part. At each iteration step we replace $\lfloor w(x)\rfloor$ of the population members with x' and a further member with probability p. In the implementation of the above algorithm we have typically used field populations of size $\mathcal{N}=25\,000$ and assumed equilibration of the algorithm after 2000 steps.

B. Simulations

In order to check the validity of our theoretical work, we performed numerical simulations of this model. To do this we needed to introduce a dynamical process on both the spins and the graph which will converge to an equilibrium distribution described by their respective Hamiltonians. One way to do this is via Glauber dynamics [22], the dynamics then automatically obey detailed balance. The transition rates between a given state and another state with a single "spin" flip (where we take spin in the broader sense to include the binary variables $\{c_{ij}\}$ and $\{J_{ij}\}$ as well as the more familiar $\{\sigma_i\}$) is determined by half the energy difference (or local field) between the two states. Defining general spin flip operators via $F_{ij}^c\Phi(c_{11},c_{12},\ldots,c_{NN})=\Phi(c_{11},c_{12},\ldots,-c_{ij},\ldots,c_{NN})$ and similarly for F_{ij}^J the Glauber rates can be written as

$$W[F_{ij}^c\mathbf{c},\mathbf{c}]=\frac{1}{2}\left\{1-\tanh\left[\frac{2c_{ij}-1}{2}\log\frac{c}{N}-\frac{n}{2}\log\langle e^{-\beta_f(2c_{ij}-1)\sigma_i J_{ij}\sigma_j}\rangle\right]\right\}, \tag{37}$$

$$W[F_{ij}^J\mathbf{J},\mathbf{J}]=\frac{1}{2}\left\{1-\tanh\left[J_{ij}K_p-\frac{n}{2}\log\langle e^{-2\beta_f\sigma_i c_{ij}J_{ij}\sigma_j}\rangle\right]\right\}, \tag{38}$$

where the angular brackets denote averages over the fast process for the given realization of the graph and bonds.

The nature of the coupled dynamics means that for each change to the graph (the slow dynamics), one must reequilibrate the spins, measure the averages as required in the above equation, and subsequently change the graph configuration again. Thus the computation effort required to equilibrate the slow system is very large compared to simulations on a given, fixed, graph. In particular, for strongly disordered graphs, where changing a single bond is expected to seriously alter the free-energy surface, it is very difficult to obtain reasonable statistics. For the simpler case of purely ferromagnetic bonds, namely for $K_p=\infty$ [or $r=e^{K_pJ}/2\cosh(K_pJ)=1$], changing any given bond implies that the new equilibrium distribution will be very close to the old one and the equilibration times will be in general, within reasonable limits. For cases of bond disorder with $r<1$, frustration effects come into play and simulations can require considerable time, even for small system sizes. With this in mind we have only focused our efforts on cases of $r=1$. We have performed simulations on systems with $N=200$, and in Figs. 2 and 4 we compare the results with our theoretical predictions. Due to the small system size, we must expect that there are persistent errors due to the relatively small system size, smearing of all phase transitions, and large error bars on any given measurement. Bearing this all in mind we feel that the results, particularly for the average connectivity, clearly support the theory.

VII. CONCLUSIONS

The study of complex networks has recently become a very popular field due to their ubiquity in nature, technology, and social interaction, where these fields are meant in a broad sense. While the statistical structure characterizing real

world networks (path lengths, degree distributions,…) and models that recreate these properties have been extensively studied from experimental measurements on real world systems, through numerical simulations and theory, understanding the behavior of networked systems based on local rules (dynamics) is still a relatively unexplored area [19]. We have presented a solvable model that examines a spin system on a small world graph with which we have probed cooperative behavior of the entire system (both of the graph and the spins). To overcome the theoretical challenge of systems evolving on disparate timescales we have focussed on the adiabatic limit; the graph evolves infinitely slowly relative to the spin variables. This allows us to treat the model using the well developed thermodynamics of replica theory, rather than having to treat the dynamics explicitly. The advantage of this approach is twofold. First, the results are exact in the thermodynamic limit in the region where replica symmetry is stable. We have not examined replica symmetry-breaking in our model, however experience suggests that it would only occur for $n<1$, at low temperatures (high values of β_f), and for some critical amount of disorder in the bonds $\{J_{ij}\}$. The second benefit of this approach is related to the relative simplicity of our present approach. We do not specify in advance the dynamics of the graph, but instead only describe it through its equilibrium energy function. Thus the resulting graph structure becomes an observable itself, rather than an object which is fixed from the start. Indeed, naive intuition may suggest that the optimal structure could have been scale free, so that ordering in the spins would have occurred at a higher temperature. It turns out that this was not the case, apparently due to entropic reasons.

ACKNOWLEDGMENTS

N.S.S. wishes to warmly thank RIKEN Brain Science Institute for their kind hospitality during the final stages of this work and the Fund for Scientific Research Flanders-Belgium. We thank A.C.C. Coolen, I. Pérez Castillo, and B. Wemmenhove for illuminating discussions.

APPENDIX A: THERMODYNAMIC EXPRESSIONS FOR NATURAL *n*

Since the replica dimension n represents the ratio of temperatures of the fast versus the slow process, it can, in principle, take any value $n>0$. In the special case where $n\in\mathrm{N}$ it turns out that both the analysis and numerical implementation of the equations can be simplified. In this appendix we will describe the key steps of this approach.

First, let us impose replica symmetry. The requirement of permutation invariance can be expressed, e.g., in the form, $X(\boldsymbol{\sigma})=X(\Sigma_\alpha\sigma_\alpha)$, for any distribution of the replicated spins, namely for $X\in\{P,U,V\}$. Since n takes only integer values here, we can implement this by considering

$$X(\boldsymbol{\sigma})=\sum_{\ell=0}^{n}\mathcal{X}(\ell)\,\delta\left[2\ell-n;\sum_{\alpha}\sigma_\alpha\right]. \tag{A1}$$

This ansatz holds for any distribution $X(\boldsymbol{\sigma})$ and in particular as $X\in\{P,U,V\}$, we define the ansatz in terms of the densities $\mathcal{X}\in\{\mathcal{P},\mathcal{U},\mathcal{V}\}$. Normalization of $X(\boldsymbol{\sigma})$ requires $\Sigma_{\ell=0}^{n}\mathcal{X}(\ell)\binom{n}{\ell}=1$.

Our self-consistent equations for $\{P,U,V\}$ (11)–(13) can now be transformed into relations between the field distributions $\{\mathcal{P},\mathcal{U},\mathcal{V}\}$. It is convenient to begin by working out an identity for the replica symmetric form of the general expression $\Sigma_{\boldsymbol{\sigma}}X(\boldsymbol{\sigma})F(\boldsymbol{\sigma}\cdot\boldsymbol{\tau})$. We insert the replica symmetric ansatz (A1) for X, use the gauge transformation $\sigma_\alpha\to\sigma_\alpha\tau_\alpha$, and introduce the representation of unity $1=\Sigma_{k=0}^{n}\delta[2k-n;\Sigma_\alpha\tau_\alpha]$, which results in

$$\sum_{\boldsymbol{\sigma}}X(\boldsymbol{\sigma})F(\boldsymbol{\sigma}\cdot\boldsymbol{\tau})=\sum_{\ell=0}^{n}\sum_{k=0}^{n}\mathcal{X}(\ell)\,\delta\left[2k-n;\sum_{\alpha}\tau_\alpha\right]\times\sum_{\boldsymbol{\sigma}}\delta\left[2\ell-n;\sum_{\alpha}\sigma_\alpha\tau_\alpha\right]F\left(\sum_{\alpha}\sigma_\alpha\right). \tag{A2}$$

We now define the set of replica indices $S=\{\alpha\in\{1,\ldots,n\}:\tau_\alpha=1\}$ and its complement $\bar{S}=\{\alpha\in\{1,\ldots,n\}:\tau_\alpha=-1\}$, which allows us to write $\Sigma_\alpha\tau_\alpha\sigma_\alpha=\Sigma_{\alpha\in S}\sigma_\alpha-\Sigma_{\alpha\in\bar{S}}\sigma_\alpha$. Isolating these last two summations via the unities $1=\Sigma_{k_1=0}^{k}\delta[2k_1-k;\Sigma_{\alpha\in S}\sigma_\alpha]$ and $1=\Sigma_{k_2=0}^{n-k}\delta[2k_2+k-n;\Sigma_{\alpha\in\bar{S}}\sigma_\alpha]$ and using the general identity $\Sigma_{\sigma_1\cdots\sigma_p}\delta[2q-p;\Sigma_{\alpha=1}^{p}\sigma_\alpha]=\binom{p}{q}$, we obtain

$$\sum_{\boldsymbol{\sigma}}X(\boldsymbol{\sigma})F(\boldsymbol{\sigma}\cdot\boldsymbol{\tau})=\sum_{\ell,k=0}^{n}\sum_{k_1=0}^{k}\sum_{k_2=0}^{n-k}\mathcal{X}(\ell)\,\delta\left[2k-n;\sum_{\alpha}\tau_\alpha\right]\times\delta[\ell+k+k_2-k_1-n;0]\times F(2(k_1+k_2)-n)\binom{k}{k_1}\binom{n-k}{k_2}. \tag{A3}$$

Using the above identity (and very similar manipulations) we can write our self-consistent equations as

$$\mathcal{U}(\ell)=\lambda_0^{-1}(n)\exp[cA_P(\ell,J)]A_U(\ell,J_0), \tag{A4}$$

$$\mathcal{V}(\ell)=\lambda_0^{-1}(n)\sum_{j=0}^{n}\sum_{k_1=0}^{j}\sum_{k_2=0}^{n-j}\mathcal{V}(j)e^{cA_P(j,J)+\beta_f J_0[2(k_1+k_2)-n]}\times\delta[\ell+j+k_2-k_1-n;0], \tag{A5}$$

$$\mathcal{P}(\ell)=\frac{\boldsymbol{\mathcal{U}}(\ell)\boldsymbol{\mathcal{V}}(\ell)}{\sum_{\ell=0}^{n}\binom{n}{\ell}\boldsymbol{\mathcal{U}}(\ell)\mathcal{V}(\ell)}. \tag{A6}$$

The largest eigenvalue, $\lambda_0(n)$, follows from the above by utilizing the normalization condition $\Sigma_\ell\binom{n}{\ell}\mathcal{U}(\ell)=1$. We have introduced the convenient shorthand

$$A_X(\ell,J)=\sum_{i=0}^{n}\sum_{j=0}^{\ell}\sum_{k=0}^{n-\ell}\mathcal{X}(i)\,\delta[i+k+\ell-j-n;0]\binom{\ell}{j}\binom{n-\ell}{k}\times\langle e^{\beta_f J[2(j+k)-n]}\rangle_J \tag{A7}$$

for $X\in\{P,U,V\}$ and $\mathcal{X}\in\{\mathcal{P},\mathcal{U},\mathcal{V}\}$, respectively.

We now turn our attention to the system's observables. First, let us work the magnetization (14) and spin-glass (15) order parameters. We substitute the replica symmetric ansatz for $P(\boldsymbol{\sigma})$ (A1) into their definitions, which together with a minor rearrangement gives

$$m=\sum_{\ell=1}^{n}\mathcal{P}(\ell)\binom{n-1}{\ell-1}-\sum_{\ell=0}^{n-1}\mathcal{P}(\ell)\binom{n-1}{\ell}, \tag{A8}$$

$$q=\sum_{\ell=2}^{n}\mathcal{P}(\ell)\binom{n-2}{\ell-2}+\sum_{\ell=0}^{n-2}\mathcal{P}(\ell)\binom{n-2}{\ell}-\sum_{\ell=1}^{n-1}\mathcal{P}(\ell)\binom{n-2}{\ell-1}. \tag{A9}$$

Let us now proceed to the observables probing organization phenomena within the graph. Here we will need the integer n representation of the transfer matrix. Inserting (A1) in (10) leads to

$$T_{\boldsymbol{\sigma},\boldsymbol{\sigma}'}[P]=\sum_{k=0}^{n}\delta\left(2k-n;\sum_{\alpha}\sigma^{\alpha}\right)e^{\beta_f J_0\boldsymbol{\sigma}\cdot\boldsymbol{\sigma}'+cA_P(k,J)}. \tag{A10}$$

After some combinatorial work, the fraction of bonds which are not energetically optimized (17) is found to be given by

$$\begin{aligned}\psi=&D_1\sum_{i=1}^{n}\sum_{j=0}^{n-1}\sum_{k=0}^{i-1}e^{\beta_f J_0(2k-j-1)}\binom{n-1}{i-1}\binom{i-1}{k}\binom{n-i}{j-k}\\&\times\{\mathcal{V}(i)\mathcal{U}(j)e^{cA_P(i,J)}+\mathcal{V}(j)\mathcal{U}(i)e^{cA_P(j,J)}\}\\&+D_2 2p\sum_{i=1}^{n}\sum_{j=0}^{n-1}\sum_{k=0}^{i-1}\mathcal{P}(i)\mathcal{P}(j)\binom{n-1}{i-1}\binom{i-1}{k}\\&\times\binom{n-i}{j-k}e^{\beta_f J[n+2(2k-i-j)]}+D_2(1-p)\sum_{i=1}^{n}\sum_{j=1}^{n}\sum_{k=0}^{i-1}\mathcal{P}(i)\mathcal{P}(j)\\&\times\binom{n-1}{i-1}\binom{i-1}{k}\binom{n-i}{j-k-1}e^{\beta_f J[n+2(2k+1-i-j)]}\\&+D_2(1-p)\sum_{i=0}^{n-1}\sum_{j=0}^{n-1}\sum_{k=0}^{i}\mathcal{P}(i)\mathcal{P}(j)\binom{n-1}{i}\binom{i}{k}\\&\times\binom{n-i-1}{j-k}e^{\beta_f J[n+2(2k-i-j)]}.\end{aligned} \tag{A11}$$

The average number of connections (18) is found to be

$$\bar{c}=c\sum_{k=0}^{n}\mathcal{P}(k)A_P(k;J)\binom{n}{k}, \tag{A12}$$

while the degree distribution (20) becomes

$$\Xi(k)\sim\frac{c^k}{k!}\sum_{i=0}^{n}\binom{n}{i}\mathcal{V}(i)\mathcal{U}(i)A_P^k(i,J). \tag{A13}$$

[1] S. Milgram, Psychol. Today **2**, 60 (1967).
[2] A. Barrat, M. Barthélemy, and A. Vespignani, Phys. Rev. E **70**, 066149 (2004).
[3] D. Y. C. Chan, B. D. Hughes, A. S. Leong, and W. J. Reed, Phys. Rev. E **68**, 066124 (2003).
[4] S. N. Dorogovtsev, and J. F. F. Mendes, Adv. Phys. **51**, 1079 (2002).
[5] R. W. Penney, A. C. C. Coolen, and D. Sherrington, J. Phys. A **26**, 3681 (1993).
[6] A. C. C. Coolen, R. W. Penney, and D. Sherrington, Phys. Rev. B **48**, 16116 (1993).
[7] T. Nikoletopoulos, and A. C. C. Coolen, J. Phys. A **37**, 8433 (2004).
[8] T. Nikoletopoulos, A. C. C. Coolen, I. Pérez Castillo, N. S. Skantzos, J. P. L Hatchett, and B. Wemmenhove, J. Phys. A **37**, 6455 (2004).
[9] D. J. Watts, and S. H. Strogatz, Nature **393**, 440 (1998).
[10] A. L. Barabási, and R. Albert, Science **286**, 509 (1999).
[11] R. Monasson, J. Phys. A **31**, 513 (1998).
[12] B. Wemmenhove, and A. C. C. Coolen, J. Phys. A **36**, 9617 (2003).
[13] B. Wemmenhove, T. Nikoletopoulos, and J. P. L. Hatchett, e-print cond-mat/0405563.
[14] L. Viana, and A. J. Bray, J. Phys. C **18**, 3037 (1985).
[15] I. Kanter, and H. Sompolinsky, Phys. Rev. Lett. **58**, 164 (1987).
[16] M. Mezard, and G. Parisi, Europhys. Lett. **3**, 1067 (1987).
[17] B. Wemmenhove, N. S. Skantzos, and A. C. C. Coolen, J. Phys. A **37**, 7653 (2004).
[18] B. Wemmenhove, and N. S. Skantzos, J. Phys. A **37**, 7843 (2004).
[19] M. E. J. Newman, SIAM Rev. **45**, 167 (2003).
[20] M. Mézard, and G. Parisi, Eur. Phys. J. B **20**, 217 (2001).
[21] J. S. Yedidia, W. T. Freeman, and Y. Weiss, in *Exploring Artificial Intelligence in the New Millenium* (Science & Technology Books, San Francisco, 2003) pp. 239–236.
[22] R. J. Glauber, J. Math. Phys. **4**, 294 (1963).